Journal of Hydrology 614 (2022) 128467

Contents lists available at ScienceDirect

Journal of Hydrology

journal homepage: www.elsevier.com/locate/jhydrol

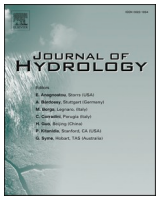

Research papers

A simple framework for calibrating hydraulic flood inundation models using Crowd-sourced water levels

Antara Dasgupta [a,b,c,*,1], Stefania Grimaldi [c], RAAJ Ramsankaran [b], Valentijn R.N. Pauwels [c], Jeffrey P. Walker [c]

[a] IITB-Monash Research Academy, Mumbai, India
[b] Department of Civil Engineering, Indian Institute of Technology Bombay, Mumbai, India
[c] Department of Civil Engineering, Monash University, Clayton, VIC, Australia

ARTICLE INFO

Keywords:
LISFLOOD-FP
Hydrodynamic modelling
Crowd-sourcing
Sensitivity analysis
Model evaluation

ABSTRACT

Floods are the most commonly occurring natural disaster, with the Centre for Research on the Epidemiology of Disasters 2021 report on "The Non-COVID Year in Disasters" estimating economic losses worth over USD 51 million and more than 6000 fatalities in 2020. The hydrodynamic models which are used for flood forecasting need to be evaluated and constrained using observations of water depth and extent. While remotely sensed estimates of these variables have already facilitated model evaluation, citizen sensing is emerging as a popular technique to complement real-time flood observations. However, its value for hydraulic model evaluation has not yet been demonstrated. This paper tests the use of crowd-sourced flood observations to quantitatively assess model performance for the first time. The observation set used for performance assessment consists of 32 distributed high water marks and wrack marks provided by the Clarence Valley Council for the 2013 flood event, whose timings of acquisition were unknown. Assuming that these provide information on the peak flow, maximum simulated water levels were compared at observation locations, to calibrate the channel roughness for the hydraulic model LISFLOOD-FP. For each realization of the model, absolute and relative simulation errors were quantified through the root mean squared error (RMSE) and the mean percentage difference (MPD), respectively. Similar information was extracted from 11 hydrometric gauges along the Clarence River and used to constrain the roughness parameter. The calibrated parameter values were identical for both data types and a mean RMSE value of ~50 cm for peak flow simulation was obtained across all gauges. Results indicate that integrating uncertain flood observations from crowd-sourcing can indeed generate a useful dataset for hydraulic model calibration in ungauged catchments, despite the lack of associated timing information.

1. Introduction

Hydraulic models have traditionally been calibrated with observations of channel flow and water depth, measured by hydrometric river gauges (Domeneghetti et al., 2014). For pluvial events where the flooding could be disconnected from the channel, gauges within the channel cannot provide useful information (Assumpção et al., 2018). Remote sensing (RS) forms part of the solution, however, hurdles such as cost and frequency of acquisition have to be fully addressed to enable routine use of RS data (Grimaldi et al., 2016). Moreover, the definition of an optimal RS-derived product (water level/flood extent) including resolution and acquisition time, as well as the definition of appropriate ways to evaluate and account for RS-derived data uncertainty, still remain a challenge and are active areas of research.

As a complement to RS or where RS data are not available, crowd-sourced data can be utilized to supplement flood information (Annis & Nardi, 2019). For example, for flash floods or fast moving floods in small catchments, the latency between satellite tasking, acquisition, and data delivery for commercial satellites, or the revisit cycles for public satellites (Lopez et al., 2020), could prove to be prohibitive, resulting in the flood wave having receded before it can be imaged (See, 2019). Consequently, novel sources of low-cost data which can be acquired frequently and in abundance are needed. Citizen science (including citizen participation up to the scientist level) or crowd-sourcing

* Corresponding author.
E-mail address: antara.dasgupta@uni-osnabrueck.de (A. Dasgupta).
[1] Now at Remote Sensing Working Group, Institute of Informatics, University of Osnabrück, Germany.

https://doi.org/10.1016/j.jhydrol.2022.128467
Received 8 March 2022; Received in revised form 15 August 2022; Accepted 1 September 2022
Available online 24 September 2022

(distributing a task among many agents), is an emerging concept in which citizens monitor the environment around them (See et al., 2016). In recent years, citizen science has provided distributed data on a variety of hydraulic variables, including water level (Kutija et al., 2014), flow velocity (Le Boursicaud et al., 2016; Le Coz et al., 2016), flood extent (Schnebele et al., 2014), topography (Shaad et al., 2016), and land-use land-cover (See et al., 2016). Furthermore, the extraction of water levels from crowd-sourced images of flooding from social media has also been automated successfully to a large extent, allowing practitioners to access often large databases of such observations previously inaccessible (e.g., Fohringer et al., 2015; Chaudhary et al., 2019; Chaudhary et al., 2020). As Nardi et al. (2021) assert in their transdisciplinary conceptual framework for citizen science in hydrology, the ubiquity of such data demands the development of novel approaches to leverage this information and reduce flood model uncertainties.

On reviewing the potential of citizen science for flood modelling, Assumpção et al. (2018) found a clear lack of appropriate techniques to utilize these data for model calibration and validation. The few studies which have examined the impact of including crowd-sourced water level data, have either used qualitative approaches (Kutija et al., 2014; Yu et al., 2016) or focused on hydrological model validation with synthetic observations (Mazzoleni et al., 2015; Mazzoleni et al., 2018). Approaches to utilize crowd-sourced observations of water level for effective model parameterization still need to be developed (Paul et al., 2018). This study demonstrates for the first time the quantitative use of crowd-sourced flood observations to parameterize a hydraulic model. Here, crowd-sourced observations of floodplain water levels were used to identify a uniform channel roughness. In simple terms, the channel roughness quantifies the resistance to the flow of water exerted by the channel per unit area, typically determined by the river bed vegetation type and density.

The primary objective of this study was to develop a simple framework to utilize water level observations from crowd-sourced data for model calibration. Calibration here implies fine-tuning the model parameters so that the simulations optimally fit the observations (Assumpção et al., 2018). The parameter values identified using crowd-sourced data were then compared with those derived from gauges, allowing verification of the parameter choice guided by crowd-sourced observations. Finally, flood extent from the calibrated model was validated against an independent optical remote sensing image acquired during the receding limb, i.e. the post-peak phase when the river water levels have reduced and the excess water has been discharged into the floodplain as overland flow.

2. Study area

The Clarence Catchment is situated in the far north coast of New South Wales. It is one of the largest river systems on the South-Eastern coast of Australia (Fig. 1), with a net drainage area of about 22,700 sq. kms. The Clarence Valley extends from 28°30′ S to 30°25′ S latitude and 152°4′ E to 153°21′ E longitude. The main stem of the river is approximately 394 km long and occupies the southern part of the Clarence-Moreton Basin in north-eastern New South Wales. The study reach from Lilydale to Yamba is approximately 164 km in length. The land cover of the Clarence region is primarily dominated by grassland vegetation and agriculture, with some urban settlements around Grafton, Ulmarra, Maclean, and Yamba. The mean annual rainfall for the basin is 1,111 mm and mean annual actual evapotranspiration is 854 mm.

The Clarence River is perennial with a mean annual flow of ~5,727 GL and a runoff coefficient of about 0.23 (NLWRA, 2000). There have been 73 major and moderate flood events since 1839, with the most recent major events recorded in 2022, 2021, 2013, and 2011 (Huxley & Beaman 2014). The largest flood on record occurred in 2013, which reached water levels of 8.09 m Australian Height Datum (AHD) at Grafton, Prince Street Gauge (Huxley & Beaman 2014). Floods in this catchment move fast, resulting in a flashy catchment response, i.e. the time lag between precipitation excesses and the associated inundation is rather short (Rogencamp 2004). For example, in 2011, the flood peak travelled from Lilydale to Yamba in less than 30 h (Grimaldi et al., 2018). Low-intensity, long-duration rainfall events are the dominant cause of flooding in the area, closely followed by the back propagation of ocean storm tides which control inundation dynamics as far upstream as Maclean (Ye et al., 1997). The catchment is characterized by flow velocities ranging from 2 to 5 m/s in the channel and the levee system, to almost zero in the backwaters (Sinclair Knight Merz & Roads and Traffic Authority of NSW, 2011). Extensive levee walls have been constructed to protect Grafton, Ulmarra, and Maclean from flooding (Rogencamp 2004).

3. Data description

The Clarence Valley Council provided field data in the form of photographs of wrack marks (debris deposited at the flood edge) and water marks (staining on the side of structures within the flooded area) some of which are available online.[2,3,4,5] These photographs were collected and interpreted visually by the council experts immediately after the 2013 event, and were provided as 32 water level observations whose timing of acquisition was unknown. Further information on the collection of the images is unfortunately unavailable to the authors or even to the council, due to personnel changes as the flood occurred nearly a decade ago, but it is clear that the images were not captured by the council but rather requested from the valley residents. The 32 interpretable photos are thus treated as "crowd-sourced" observations here and used for hydraulic model calibration (shown in Fig. 2 alongside example photos). Interpreting water levels from crowd-sourced field photos of flooding is out of scope for this manuscript, however, recent advances in deep learning suggest that automatic derivation at scale could be possible soon (e.g. Chaudhary et al., 2020).

It is worth noting that a much larger number of photographs were available to the council (145), but only 32 of these turned out to be useful for the interpretation of water levels. The conundrum of available vs usable data is representative of any crowd-sourcing based data collection exercise, where the available data quantity typically exceeds the amount of actually usable data. However, studies have demonstrated the value of including even a few independent crowd-sourced points (e.g. 20–50) to improve the quality of flood mapping from satellites by providing complementary information on flood inundation (see Sunkara et al., 2020 for further details). Furthermore, many of the residents of the Clarence area had recently lived through record flooding in 2011, which may have contributed to their understanding of some flood processes and in turn influenced the quality of the submitted photographs. It could be argued that these many observations or the data collection procedure, are not enough to be qualified as "crowd-sourced" data, which is typically characterized by larger data volumes. However, on considering the acquisition and collection techniques described above, the dataset is classified as crowd-sourced and not a citizen science

[2] https://www.flickr.com/photos/50615476@N03/8503268526/in/pool-abcnorthcoast/.
[3] https://www.facebook.com/GraftonAustraliaFloods2013/about/?ref=page_internal.
[4] https://www.dailytelegraph.com.au/news/nsw/grafton/floods-maclean-Tuesday-January-29–2013/image-gallery/744379f7b46246989ec0a7133346cbb9.
[5] https://www.dailytelegraph.com.au/news/nsw/grafton/floods-yamba-Wednesday-January-30–2013/image-gallery/2e101b950af514999f487beffccb3b97?page=4.

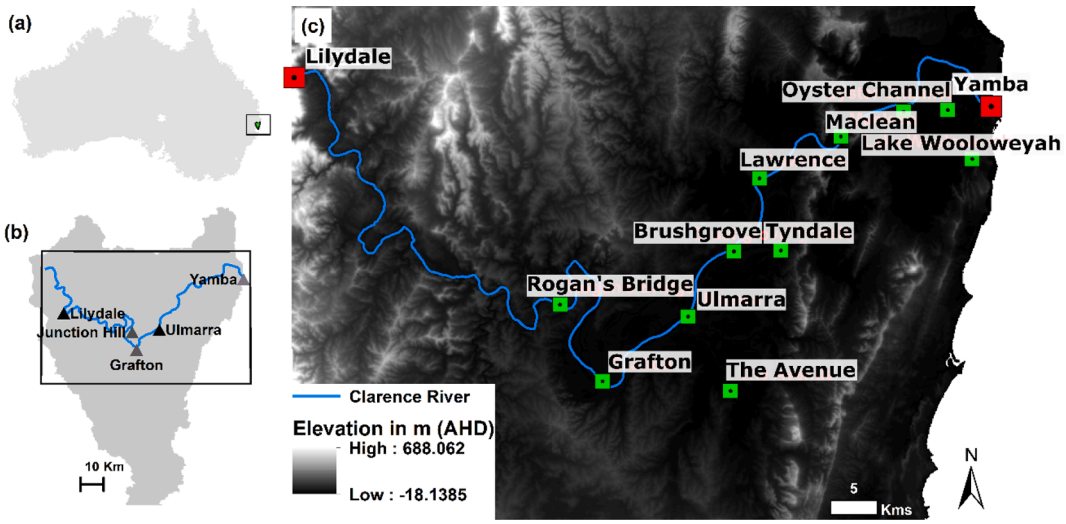

Fig. 1. Geographical location of the Clarence Catchment, Australia shown in (a), with the Clarence River and nearby towns marked with respect to the Clarence River Catchment in (b). The extent of the model domain from Lilydale to Yamba is shown in (c), with model boundary conditions marked in red squares while gauge locations are represented by green squares. The LiDAR DEM made available by Geoscience Australia is displayed as the base layer. (For interpretation of the references to colour in this figure legend, the reader is referred to the web version of this article.)

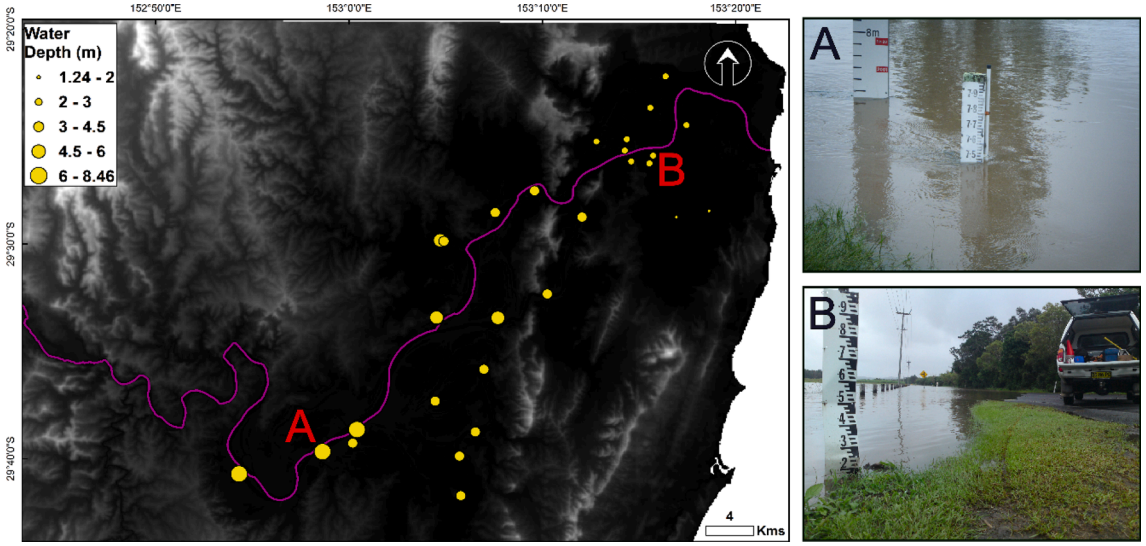

Fig. 2. Locations of the "crowd-sourced" water depth observations for the 2013 flood event in the Clarence Catchment. Sub-figures A and B show example images used for the depth calculation, interpreted and provided by the Clarence Valley Council.

dataset, since the engagement with the citizens only extended to requesting any/all event photos.

Hydrometric gauge information was provided by the NSW Public Work's Manly Hydraulics Laboratory (MHL) and the Australian Bureau of Meteorology (BoM). The observations were recorded with a temporal frequency of fifteen minutes for the WL gauges. Missing data were interpolated using linear interpolation for WL observations available at Rogan's Bridge, Grafton, Ulmarra, Brushgrove, Lawrence, Maclean, Palmer's Island Bridge, and Yamba, from upstream to downstream along the main stem of the river. Gauge locations are shown in Fig. 1, while hydrographs recorded by gauges along the main stem of the channel are shown in Fig. 3 for the 2013 flood event. Additionally, WL observations were available at Tyndale, The Avenue, Oyster Channel, and Lake Wooloweyah. The WL values were recorded in meters with respect to AHD and used to verify the channel friction parameter identified using crowd-sourced observations.

Topographic information was available in the form of a 1 m Light Detection And Ranging (LiDAR) bare earth Digital Elevation Model (DEM), acquired between 2001 and 2015 with a vertical accuracy of ±30 cm and horizontal accuracy of ±80 cm (DFSI, 2010; Fig. 4). This dataset is freely available under a Creative Commons Attribution 4.0 license, for commercial and non-commercial applications at https://elevation.fsdf.org.au/, provided by Geoscience Australia. The channel bathymetry was reconstructed by interpolating between field-observed cross-sections and stitched to the LiDAR DEM, for the part of the domain where it was available. Bathymetric data were collected during a field campaign in 2015 described extensively in Grimaldi et al. (2018), and supplemented with pre-existing bathymetric datasets (Farr & Huxley 2013). The area upstream of Copmanhurst where LiDAR coverage was unavailable, was in-filled with the SRTM-derived 30 m product.

An optical multi-spectral image from the Satellite Pour l'Observation de la Terre (SPOT) 6 satellite was available to this study (Fig. 4), acquired on January 31, 2013 at 09:35 AM (AEDT). The data were acquired at 6 m resolution and delivered as an *ortho*-rectified, pan-sharpened multi-spectral (PMS) product at 1.5 m with four spectral

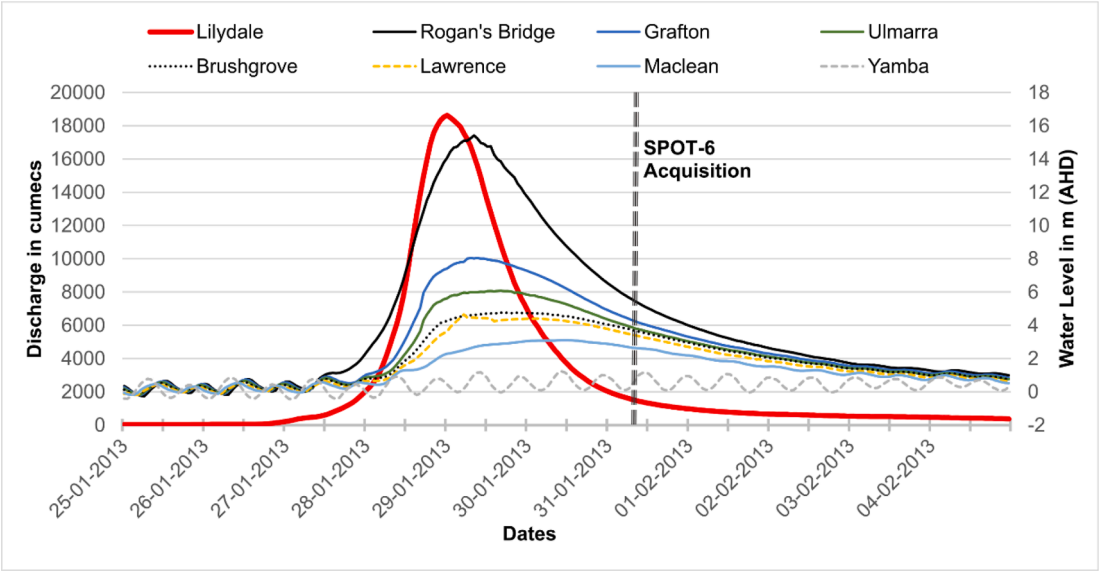

Fig. 3. Hydrographs recorded at the hydrometric gauges along the main stem of the Clarence River (locations shown in Fig. 1) for the 2013 flood event, shown together with the temporal acquisition of available remote sensing data. The shaded hydrograph refers to the inflow boundary condition at Lilydale.

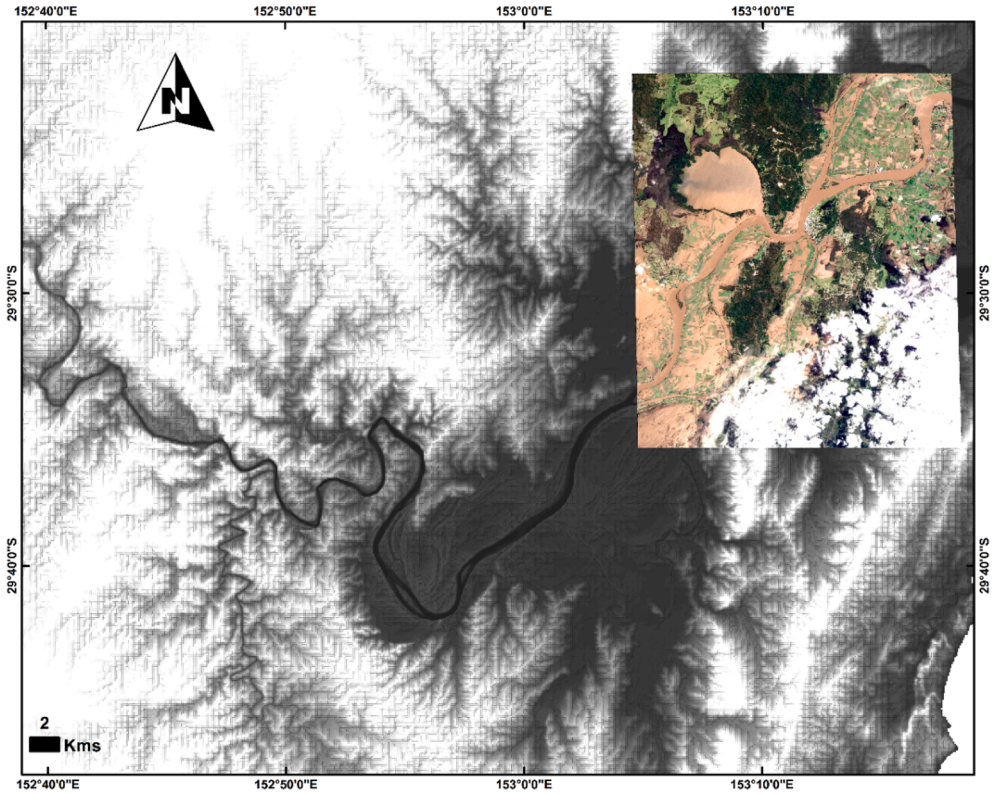

Fig. 4. Spatial extent of the SPOT-6 optical image covering the 2013 flood event in the Clarence, shown here with respect to the model domain. The LiDAR DEM available to this study is used as the base layer.

bands, i.e. blue (450–520 nm), green (530–590 nm), red (625–695 nm), and near infrared (760–890 nm). SPOT-6 PMS products have a radiometric resolution of 12 bits per pixel and the image was delivered in the JPEG 2000 raster format (Astrium Services 2013). The image comprised of a total of 250 million pixels covering a total area of 573.91 km^2. About 25 % of the tile was affected by cloud cover, obscuring the underlying inundated regions. In order to avoid the associated uncertainty, this portion of the image was removed from the analysis.

Fig. 4 shows the spatial extent of the SPOT image with respect to the model domain, along with the temporal position with respect to the 2013 flood hydrographs. This image was converted to Normalized Differential Water Index (NDWI) (McFeeters, 1996) values to delineate the flood waters. The true colour composite of the SPOT image is juxtaposed against the derived NDWI image in Fig. 6. Problems of flood monitoring using optical data are apparent, as nearly 25 % of the image is unusable due to cloud cover. Although the initial formula for the calculation of NDWI was developed for applications to the Landsat Multi Spectral Scanner (MSS) sensors, it has since been extended to all optical satellites

(McFeeters, 2013). The general equation used for calculation of NDWI in this study is given as.

$$NDWI = \frac{Green - NIR}{Green + NIR} \quad (1)$$

where NIR refers to the Near-Infrared channel.

4. Methods

The overall methodology for this component of the research is summarized in Fig. 5.

4.1. Model implementation

The LISFLOOD-FP inertial acceleration solver was implemented in full 2D for the Clarence Catchment at 30 m grid resolution, as Grimaldi et al. (2018) found it a cost-effective modelling solution for the Clarence Catchment. Implementation of this model requires a DEM, river geometry information, boundary conditions, and channel/floodplain roughness values which can be specified as lumped or distributed. For the floodplain, spatially distributed roughness values were assigned based on Arcement & Schneider (1989) recommendations for given land-uses, which in turn were assessed using field and aerial photographs. This spatially distributed floodplain roughness map was used consistently throughout this study, for all the "lumped" channel roughness calibration experiments. The only exception from this are the floodplain roughness tests described in Section 4.2. The discharge measurements available at the Lilydale gauging station were used as the upstream boundary (Neumann condition). Tidal water levels observed at Yamba were similarly used as the downstream boundary condition (Dirichlet condition), see Fig. 1 for the locations of Lilydale and Yamba, which form the boundaries of the study reach. Lateral inflows were not included in the model setup, as they did not contribute significant water volumes during the 2013 flood event, which was dominated by a combination of high rainfall and tidal levels (Rogencamp 2004).

Using tidal water levels as the downstream boundary, additionally allowed the evaluation of backwater effects on floodplain inundation for this catchment. Most hydraulic modelling studies choose to disaggregate spatially distributed coefficients of channel and floodplain roughness, into just one spatiotemporally invariant value for each (Werner et al., 2005). These are generally considered as effective parameters in hydraulic modelling, used to compensate for inadequate process and topographic representation (Horritt & Bates 2001; Jung et al., 2012). The floodplain roughness parameter is expected to be sensitive only during high velocity out-of-bank flows, as water shear will dominate resistance to flow once the floodplain is already wet (Mason et al., 2003; Schumann et al., 2007). As the events analysed in this paper were between 20 and 30 year return period floods, distributed time invariant values of floodplain roughness were assigned based on the land-use and kept constant for all runs.

4.2. Model calibration

Channel roughness is the only calibration parameter for this particular model implementation, which primarily controls the flood wave arrival time. Here, a lumped Manning's n value for the channel was optimized from 0.020 to 0.035 s/m$^{1/3}$, which is the seasonal range of values for the Clarence River, by varying it in increments of 0.001 s/m$^{1/3}$ (Farr & Huxley 2013). This range was selected based on preliminary tests whereby a well-performing range was selected for further refinement of the model. Starting with 32 uniformly spaced Manning's n values, within the range of possible values for the channel friction (0.01 to 0.1 s/m$^{1/3}$), the hydraulic model was run using a distributed land-use based floodplain roughness map. The channel roughness range was selected according to the Kling-Gupta Efficiency (KGE; Gupta et al., 2009) as calculated for a few select gauges and the Mean Absolute Bias (MAB) and Root-mean-squared-errors (RMSE) for the CS data points. In each iteration 32 uniformly spaced values within the range were evaluated, and the best performing range of roughness values selected for the next iteration with finer increments. Fig. 7 shows the plots from the parameter range refinement exercise, with subplots (a), (b), and (c), showing the outcomes from the three iterations for channel roughness, and (d) for the floodplain roughness. The left-axis shows the KGE values and the right axis shows the RMSE, while the different coloured lines show the objective function values.

As these were "crowd-sourced" observations of high water marks, it

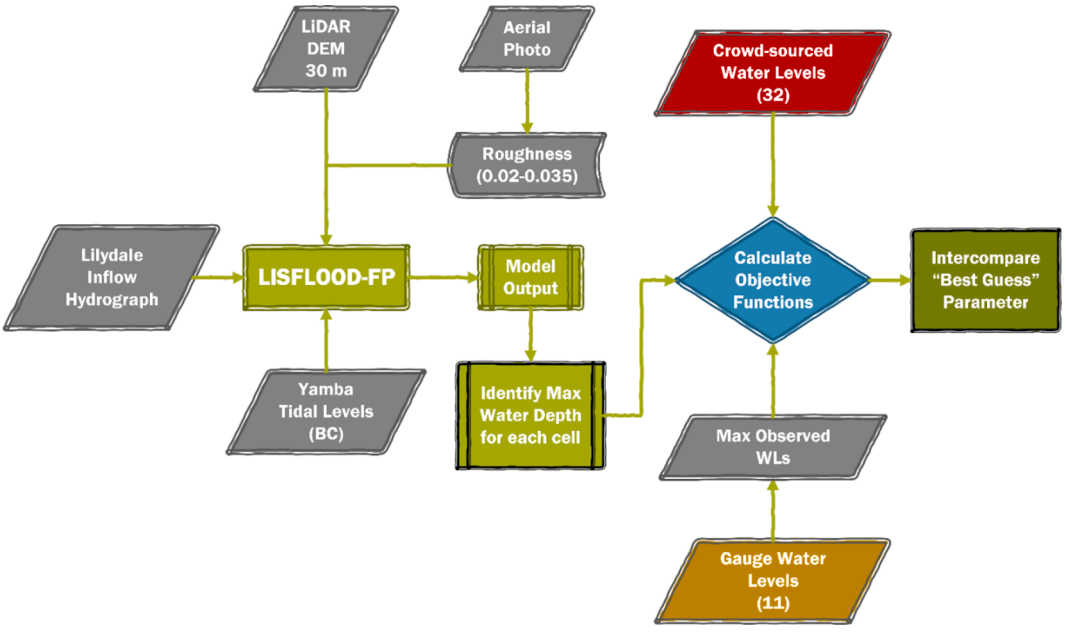

Fig. 5. Schematic of overall methodology used in this paper for the parameterization of channel roughness in LISFLOOD-FP. The number of "crowd-sourced" and gauged water level locations has been included in the illustration, along with the range of roughness values considered for calibration which were identified from aerial field photographs. BC = Boundary Conditions; WLs = Water Levels.

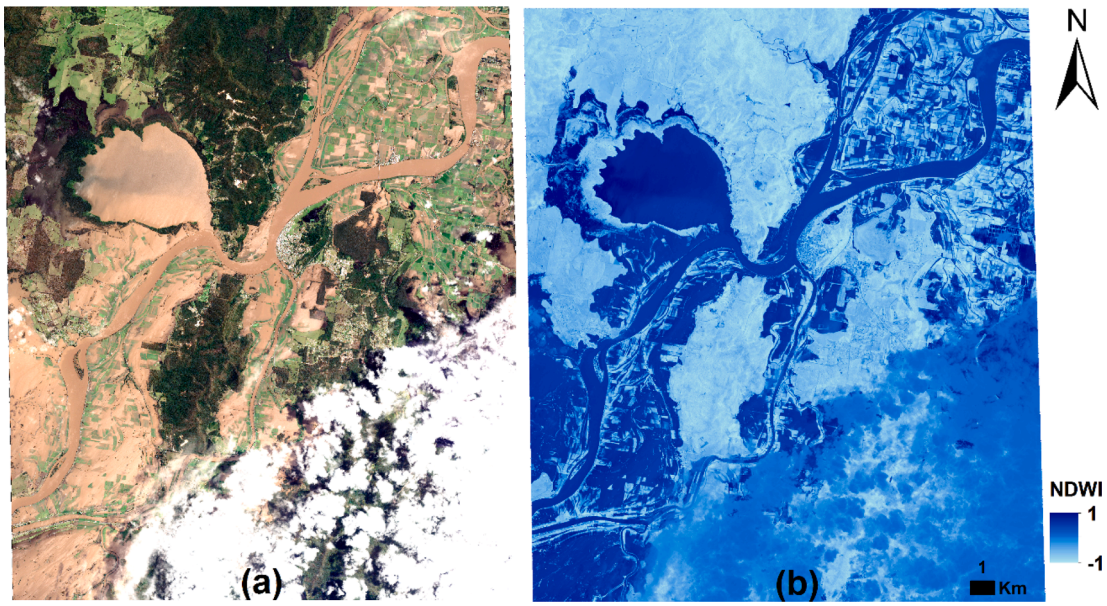

Fig. 6. Optical multispectral imagery from the SPOT-6 satellite, with (a) showing a true colour composite of the area, and (b) showing the Normalized Differential Water Index values derived from (a).

is reasonable to assume that they coincided with the peak flow recorded at the nearest river gauging station. In the absence of adequate information on the data acquisition procedures, this assumption was based on multiple previous studies where HWMs were assumed to correspond to the simulated maximum water levels (see for example Di Baldassarre et al., 2009; Prestininzi et al., 2011). For each model grid cell where a corresponding crowd-sourced observation was available, the simulated maximum water depth (MWD) was first evaluated. Subsequently, the two chosen objective functions, the Root Mean Squared Error ($RMSE_{MWD}$) and Mean Percentage Difference (MPD_{MWD}) were calculated. The metrics were calculated by comparing the simulated maximum water depth (Sim_{MWD}) for each model grid cell coinciding with a crowd-sourced or gauge observation (i), against the crowd-sourced/gauged value (Obs_{MWD}), and then averaging across all observations (m). The RMSE was chosen to quantify absolute error in the simulation, while the MPD function allowed a relative error assessment with respect to the observation values. The objective functions were computed as.

$$RMSE_{MWD} = \sqrt{\frac{\sum_{i=1}^{m}(Sim_{MWD} - Obs_{MWD})^2}{m}} \tag{2}$$

$$MPD_{MWD} = \frac{Abs(Sim_{MWD} - Obs_{MWD})}{Obs_{MWD}} \times 100 \tag{3}$$

$$MinE_{opt} = \min_{j}(RMSE_j^{MWD} \times \left|MPD_j^{MWD}\right|) \tag{4}$$

Here j refers to a specific roughness value and J refers to the complete set of roughness values evaluated herein, over which the minima is calculated. The roughness value corresponding to the minima of the product ($MinE_{opt}$) of $RMSE_{MWD}$ and MPD_{MWD}, was selected as the best performing parameter n_{opt} from all the tested roughness values. The product was considered as it is a simplified approach towards multi-objective optimization, as both objective functions needed to be minimized. Furthermore, the product was chosen over the sum as it further inflates the objective function values, amplifying the variability captured by the metric and helping to differentiate between models with only slight differences in performance. As the information content of the observations is distributed in space but limited in time, it is postulated that using more than one objective function with different priorities will allow for a more robust evaluation (Zhang et al., 2013). Best fit parameters identified by using crowd-sourced and gauged water levels (using only the flood peak value, since it was the only information consistently available across all data sources), were inter-compared to assess the information content of the crowd-sourced data. The maximum water depth values computed by the numerical model were finally compared with crowd-sourced and gauged water levels to arrive at the calibrated parameter value.

4.3. Model validation

Parameter values chosen through the procedures outlined in the previous section were additionally verified using NDWI values from an independent optical remote sensing dataset, to ensure reliability of the simulated inundation patterns. NDWI uses features of the water reflectance spectrum, i.e. maximum reflectance in the green region of the electromagnetic spectrum and minimum in the NIR region, to enhance the identifiability of water surfaces. It also exploits the high reflectance of terrestrial vegetation and soil in the NIR region to aid the delineation of water bodies (McFeeters, 1996). While using a band ratio approach for surface water detection does not eliminate uncertainties (Mukherjee & Samuel, 2016); the objective here was just to achieve an acceptable model set up, which was considered sufficient to verify the parameter choices (Andreadis & Schumann, 2014).

NDWI values larger than 0 are typically expected to represent water pixels, while negative values represent non-water land-use classes (Jain et al., 2005; Lu et al., 2011). Accordingly, the cloud-free portion of the SPOT image was processed to derive NDWI values, which was subsequently converted into a surface water map using a global threshold of 0 to retain positive values. NDWI values were derived from the SPOT image at the native resolution (1.5 m) of the pan-sharpened product, although these had to be upscaled to the model grid size of 90 m prior to making any comparisons. Model simulated water depths were extracted at the time of acquisition of the SPOT image and converted to inundation extent maps using a threshold of 1 cm. This depth threshold was used to derive flood extents throughout this paper. Although some studies have justified the use of a 10 cm depth threshold for reasons of uncertainty (Pappenberger et al., 2007b), it also means that a pixel with 9 cm water depth will not be considered inundated. This implies that 729 cubic meters of model simulated water volume per pixel was ignored during the flood extent assimilation process. Consequently, a threshold of 1 cm

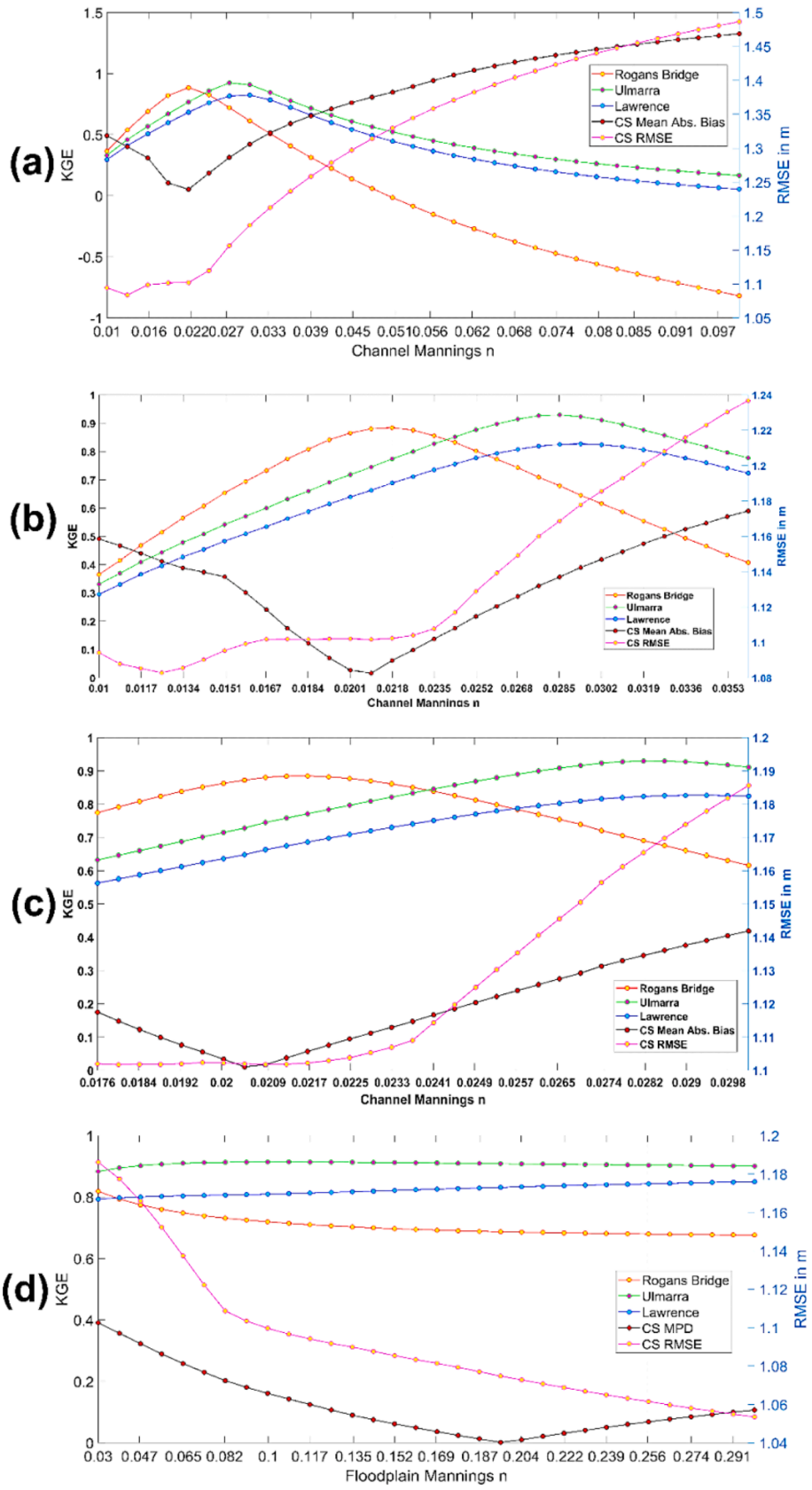

Fig. 7. Plots showing the iterative parameter range refinement exercise, with (a), (b), and (c) showing the impact of changing the channel Manning's roughness on the Mean Absolute Bias (MAB) and Root Mean Squared Errors (RMSE) for all the crowd-sourced points and the Kling Gupta Efficiency (KGE) for a few selected gauges. A similar analysis for the floodplain friction is shown in (d). Note that all lines are plotted on the primary axis (KGE), even the black line for the MAB of the CS points, with the exception being the pink line for the CS observations' RMSE plotted on the secondary axis. (For interpretation of the references to colour in this figure legend, the reader is referred to the web version of this article.)

was considered more suitable in this study (Hostache et al., 2018).

Finally, the calibrated model performance was quantified through contingency maps and confusion matrix-based performance measures. The confusion matrix is composed of four values, which in this study were defined as follows: the number of pixels correctly simulated as flooded (hits), the number of pixels simulated as flooded but dry in the observation (false alarms), the number of simulated dry but flooded in the observation (misses), and the number of pixels correctly predicted as non-flooded (correct rejects). The critical success index (*CSI*; Donaldson et al., 1975), and Cohen's kappa (Cohen, 1960) were used, as they are commonly used for binary pattern matching (Stephens et al., 2014). The performance measures were calculated as.

$$CSI = \frac{hits}{hits + misses + falsealarms} \tag{5}$$

$$Kappa = \frac{2 \times (hits \times correctrejects - misses \times falsealarms)}{(hits + falsealarms) \times (falsealarms + corectrejects) + (hits + misses) \times (misses + correctrejects)} \tag{6}$$

The critical success index corrects for the over-representation of the correct rejects in the model domain, while the kappa coefficient corrects for expected chance agreement. These metrics quantify goodness of fit; they attain their highest value of 1 when the predictions provide a perfect fit to the observations.

Due to the limitations of optical satellite imagery, which is unable to penetrate vegetation canopies and is thus incapable of detecting flood waters under vegetation. Accordingly, the Normalized Differential Vegetation Index (Wang et al., 2011), was also computed for the SPOT-6 image, to verify whether the binary mismatch between the model and the satellite observation was caused by actual disagreement or the inability of the sensor to map inundation. NDVI leverages the difference in the spectral response of the chlorophyll-loaded vegetal tissues in the red and infra-red channels of multispectral satellites, which higher values indicating high density and typical values ranging from 0.1 to 0.7 for vegetated areas (Jarlan et al., 2008). While there is no clear consensus in literature on the lower bound of NDVI values for vegetation or at which vegetation density optical sensors become unusable, investigating these questions was outside the scope of this manuscript. Here the general threshold of 0.1 to identify vegetation is used as a threshold, since the NDVI is only used as a reference to facilitate a qualitative assessment of the model validation.

5. Results and discussion

5.1. Model calibration

This section presents the results obtained from this novel calibration exercise based on crowd-sourced data and discusses the possible implications of this analysis. First, the model simulations of maximum water depth for different channel roughness values were compared with the crowd-sourced observations. Consequently, the maximum water level values for each cell containing a water mark were compared with the maximum value within the corresponding grid cell for the flood inundation model simulation. In other words, the timing of the maximum water level was not considered, which may impact the accurate simulation of the flood wave arrival and travel times. Since water level values represent the sum of the flood water depth and the underlying DEM, the vertical uncertainty in the DEM could influence the calibration

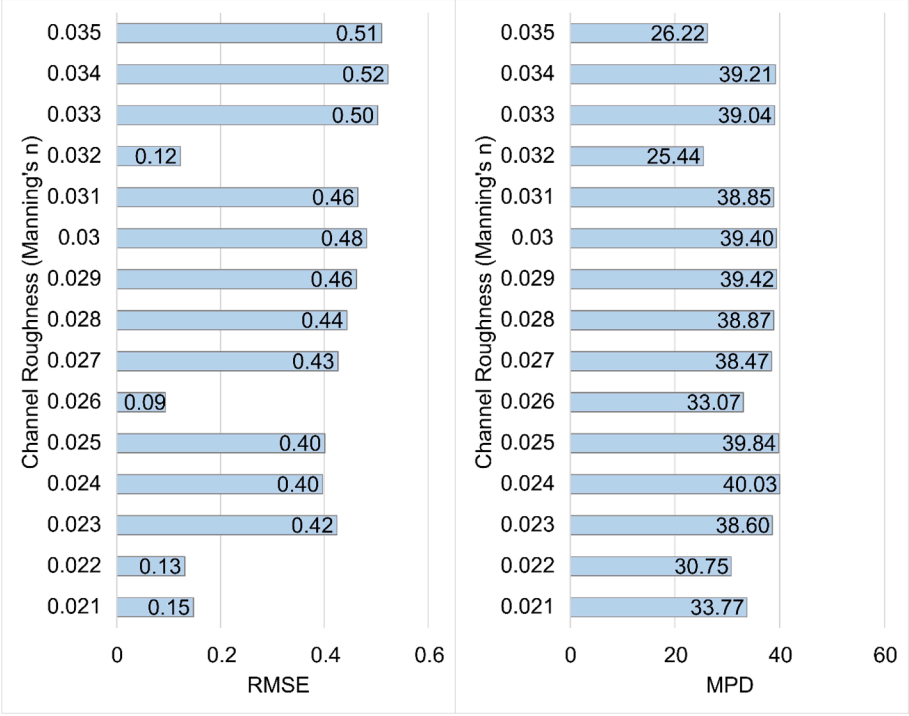

Fig. 8. Maximum water levels simulated by LISFLOOD-FP compared with crowd-sourced observations, with the plot on the left showing the root mean squared error (RMSE) values and the mean percent difference (MPD) values on the right.

outcomes. Indeed, it is possible to obtain positive/negative errors for all the simulations due to DEM uncertainty. However, the impact of the DEM uncertainty was not explicitly investigated in this study as the focus was on the use of crowd-sourced water levels for model calibration.

Fig. 8 shows the distribution of the RMSE and MPD values for the considered range of the channel roughness parameter, as compared to the crowd-sourced water level values. In this study, spatial variability in the roughness parameter was not considered, since adequate data to resolve grid-wise parameters in two-dimensional space were not available. Moreover, hydraulic model uncertainties in the forecast mode are predominantly a function of topography and inflows (Andreadis & Schumann 2014) as previously discussed. Consequently, the impact of spatial heterogeneity in the roughness characterization was not expected to yield notably different results (Giustarini et al., 2011).

The maximum RMSE across the 15 simulations within the selected "optimal" range of Manning's values was ~0.5 m and the maximum MPD ~ 40 %, which could be the reason for the low variability of the model performance. Hostache et al. (2009) reported ±40 cm RMSE through traditional calibration using a downstream limnigraph, where a LiDAR DEM with ±15 cm and observed cross-sections with up to ±30 cm uncertainty were used. The variation observed across the values of RMSE and MPD for the evaluated roughness range implies high parameter sensitivity. As the channel roughness controls the flood wave arrival time and the time of channel over-topping to some extent, which in turn influences flood plain water levels, the observed sensitivity was expected despite these factors not being explicitly considered.

The variation in the objective function values display no particular trend. Manning's n values of 0.026 and 0.032 seemed to perform well across both metrics, with RMSE values of 9 and 12 cm, respectively, and MPD values of 33.07 % and 25.44 %, respectively. Based on the multi-objective performance evaluated from Fig. 8, $n = 0.026$ was clearly the better choice, in comparison to the crowd-sourced water level observations. This choice is driven by the low absolute errors (RMSE) observed for this roughness value which compensate for the relatively higher value of relative errors (MPD), due to the nature of the objective function which is designed as a product.

The objective function values at $n = 0.026$ are substantially lower than the neighbouring Manning's values tested suggesting that it could be a local anomaly. One of the reasons for this could be the use of a uniform channel roughness value and the spatial distribution of the crowd-sourced points being skewed towards the downstream part of the catchment. Due to the uneven distribution, the calibration process will inevitably prioritize those effective parameterizations, which best simulate the inundation dynamics in this region. It is thus possible that those roughness values which best reproduced the channel over-topping time and the superposition of the tidal and flood waves in this region would be selected using the methods proposed here. This value can also be a local minima as observed from Fig. 8, as the crowd-sourced points are only able to provide information on the floodplain in the lower part of the catchment (Pappenberger et al., 2005). Moreover, the distribution of the points is sometimes really close to the channel, e.g. the points at Grafton or sometimes really far out into the floodplain, which would mean that an effective roughness value that performs equally well at both locations must be identified (Mukolwe et al., 2016). Perhaps this is not the case for the neighbouring values thus resulting in notably lower RMSE values for $n = 0.026$. Due to the nature of the hydraulic model uncertainties and the equifinality of model parameters, it is possible that a local minima best compensates for localized bathymetric errors, for instance (Beven 2006).

In contrast to the previous comparison with crowd-sourced water levels, there is a clear trend in the objective function values when inter-comparing the simulated maximum water level values with the gauged observations shown in Fig. 9. Here, the modelled and measured maximum water levels at the gauge locations were inter-compared regardless of the information on the timing of the flood peak. The values of both error metrics first increased with a corresponding increase in the magnitude of the channel roughness, then decreased after the optima. The maximum RMSE across all simulations was ~ 78 cm and the maximum MPD ~ 17 %, again indicating a suitable model setup. These findings are aligned well with the expectations; as the water depth in the channel is larger, the corresponding RMSE or the absolute error is higher. Low values of the MPD imply that the percentage error was actually lower than what was observed in the previous test against

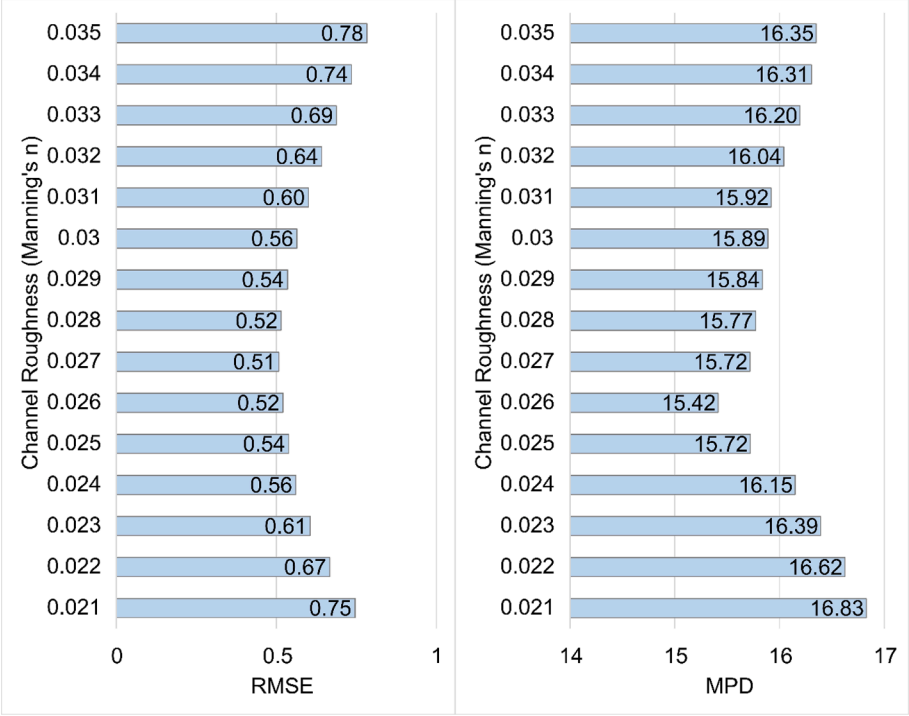

Fig. 9. As for Fig. 8 but for the maximum water levels simulated/observed at gauge locations.

crowd-sourced water levels in the floodplain. Moreover, the variability in both absolute and relative errors was lower than in the case of crowd-sourced water levels. Again, this was expected as the water level variation within the confines of the channel might not be as much as is possible in the floodplains.

In this experiment, Manning's n values between 0.025 and 0.028 seemed to perform well across both error metrics. Upon further examination of the two objective functions, $n = 0.026$ appeared to be the clear choice again. The trend observable in Fig. 9, where a nearly concave response to changes in the roughness values can be observed for both absolute and relative errors based on the objective functions, with a clearly global minima detected at $n = 0.026$. This finding corroborates the hypothesis that the Manning's roughness value selected based on Fig. 8 was a good overall fit for the channel, and the apparent "local minima" is simply an artefact of the calibration prioritizing model accuracy primarily in the downstream region. In order to further investigate the impact of the spatial distribution and outliers on the evaluated objective functions, the MPD and bias values for the two well-performing parameter choices in case of the crowd-sourced data were plotted in Fig. 10 and Fig. 11, respectively.

For the MPD maps in Fig. 10, the channel roughness value of Manning's $n = 0.026$ shown in (a) was driven by a small number of highly erroneous points (darker shades of red) towards the downstream end of the model domain and in the storages southeast of Grafton. Conversely, the MPD values for channel roughness corresponding to $n = 0.032$ shown in (b), exhibit larger errors in general (low number of light coloured points, with most in medium to dark hues). Similar trends can be observed in the maps shown in Fig. 11, showing the bias in simulated water depth where the direction of the bias in the model is also evident. Generally, the model over-predicts the water levels closer to the channel and under predict them further in the floodplains. A channel roughness value of $n = 0.026$ in (a), mostly overestimates the WLs at the first glance (lots of blue points), but a closer look reveals that a large number of points are within ±10 cm (white points), while others are still in lower error categories. In (b), a friction value of $n = 0.032$ led mostly to large positive (dark blue points) or negative errors (dark red points), with the number of low error points being very low. This analysis further confirmed the choice of channel roughness as $n = 0.026$, as it produced a more consistently accurate performance across the domain.

Despite the acceptable quality of the fit, the positive MPD values obtained in both experiments implied that the model consistently underestimated the water levels at the gauges and at the crowd-sourced observation locations in the flood plain. The magnitude of underestimation increased with distance from the channel, which could in part be related to errors in the bathymetry. Only the meandering portion of the channel between Copmanhurst and Mountainview, upstream of Grafton was surveyed recently (in 2015). It thus seems plausible that the model simulations at the crowd-sourced observation locations further downstream, were strongly impacted by the poorer quality bathymetry information. Indeed, the bathymetry downstream of Grafton until Brushgrove was surveyed in the 1960s and extrapolated further downstream using a local along-thalweg curvilinear interpolation (Grimaldi et al., 2018). Moreover, the accuracy of the bathymetric survey in this area or the interpolation were unknown, and therefore cannot be used to further diagnose the model performance here.

Given that channel bathymetry is a highly dynamic geomorphological feature which alters with changes in the flow regime or even large flood events, it is expected that the 1960s datasets could misrepresent the channel geometry. In order to obtain a better fit to the observations, distributed friction values might be required to adequately replicate the flow patterns in the downstream portion of the catchment. However, since the fit was adequate (mean RMSE ~ 50 cm), a lumped value was considered sufficient to answer the research questions posed in this study, where the aim was to assess the utility of crowd-sourced observations for hydraulic model calibration.

5.2. Best-fit parameter verification

From this investigation, it was concluded that the best performing value for the channel roughness parameter was $n = 0.026$, which was chosen for further verification. Fig. 12 and Fig. 13 show plots of the simulated and observed water depths, for crowd-sourced and gauged data points, respectively. When examined in a distributed fashion there was no clear trend in the discrepancies between modelled and observed values from upstream to downstream (gauge locations are shown in Fig. 1), i.e. the model sometimes overestimated and sometimes underestimated the measurements. Due to the relatively flat geomorphology of the region, larger values of water depth were observed within the channel associated with higher error magnitudes as expected; conversely the error magnitudes were lower in the floodplain where elevation values are lower. The MPD was generally higher for the crowd-sourced points, as even low magnitude errors constitute a large percentage of the shallow observed water depth, while the opposite was true for the gauge-based assessment within the channel.

Interestingly, these experiments show that in the absence of gauge information, crowd-sourced water level observations can provide sufficient information to calibrate a hydraulic model. However, this might only be true for the present case study and in the floodplains, as in the presence of a levee system, a-few-cm error in water level predictions can also cause false alarms/misses (Wing et al., 2017). In this context, there were still quite large discrepancies between gauged and modelled peak levels and perhaps the Nash-Sutcliffe efficiency (or other metrics) using the full hydrograph, would have allowed a more comprehensive evaluation of model accuracy. However, the objective of this experiment was to evaluate the potential of crowd-sourced data for model calibration, assuming a severely data limited scenario which may well be the case for

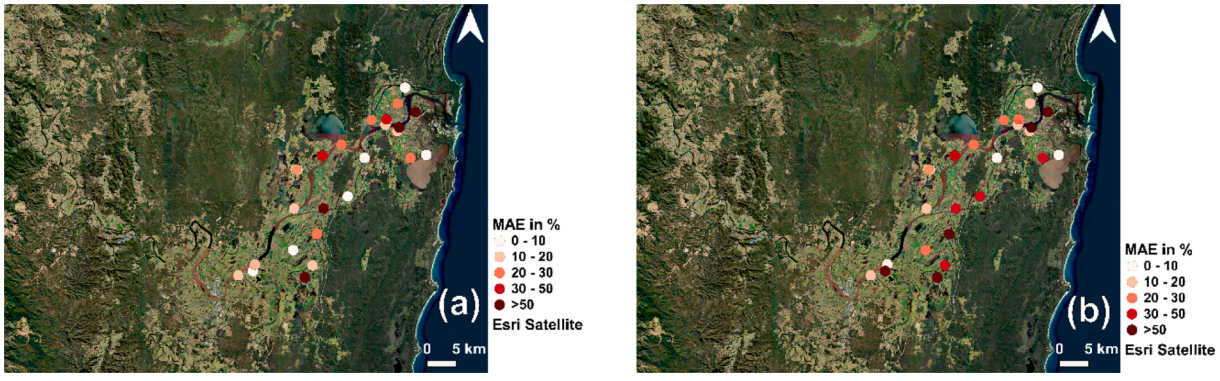

Fig. 10. Maps of the model domain showing the spatial distribution of the crowd-sourced points and the corresponding mean absolute error percentages for simulated water levels produced by using a channel friction value in Manning's n of (a) $n = 0.026$ and (b) $n = 0.032$.

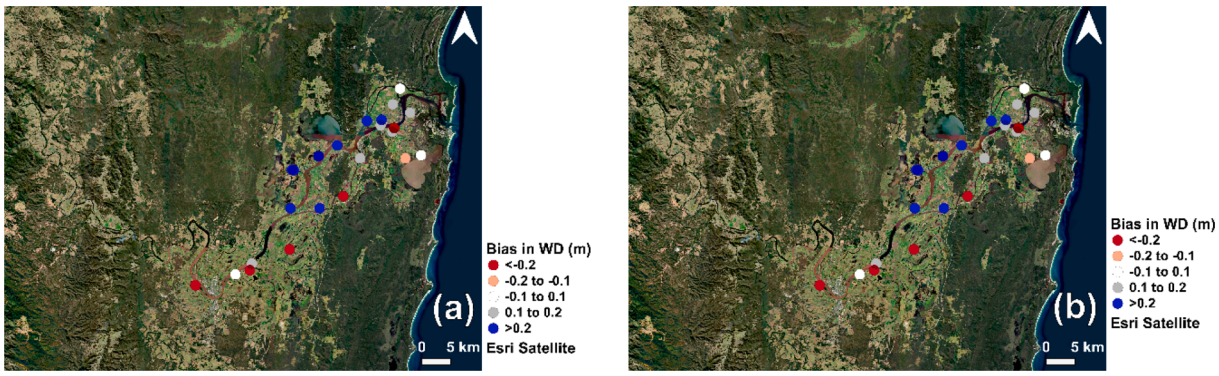

Fig. 11. As for Fig. 10, but for bias in water depth (m).

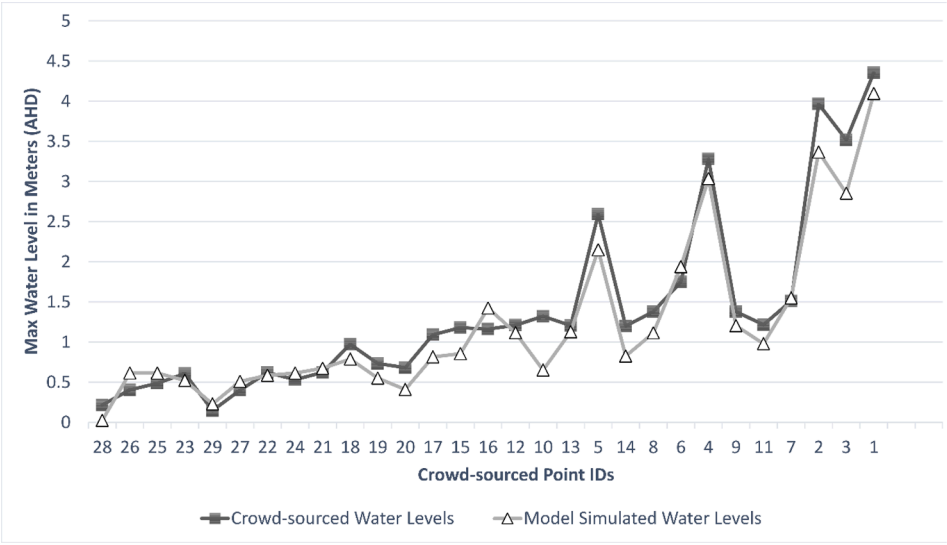

Fig. 12. Plot showing the maximum water levels simulated by the calibrated model using $n = 0.026$ and the crowd-sourced maximum water levels at all the available locations. Crowd-sourced point locations have been arranged from upstream to downstream.

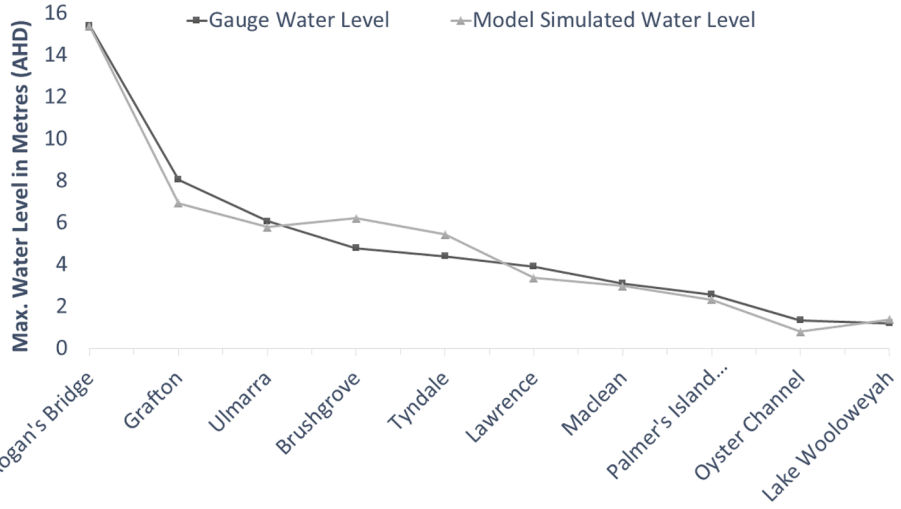

Fig. 13. Plot showing the maximum water levels simulated by the calibrated model using $n = 0.026$ and the gauged maximum water depths at all the available locations. Gauges are ordered from upstream to downstream.

most operational applications.

The number of crowd-sourced observations available to this study (32) was low compared to the huge volumes of data expected from citizen science. However, these 32 high water marks were highly accurate, while real crowd-sourced data might be affected by larger uncertainties. As natural language processing and object extraction

methods become more sophisticated, the processing of text and images/videos from social media for water level extraction is expected to be automated. If a large number of crowd-sourced water level observations with a time stamp were made available, the present methodology could be extended to accommodate those (Kutija et al., 2014), yielding further improvement in parameterization accuracy. As water level extraction techniques are automated and data volumes expand, model calibration may become more challenging as the inherent uncertainties and errors in the data and information extraction algorithms become unavoidable. In this case, the proposed methodology must be adapted to deal with this additional uncertainty, especially in the absence of complementary calibration data. One approach could be to use statistical techniques such as bootstrapping (e.g., Tellman et al., 2022), to cyclically select subsets of data and assessing their ability to resolve the model parameters, such that highly uncertain outliers can be identified and discarded. Furthermore, weighted calibration techniques may also be used if the associated uncertainties are provided by the data providers or algorithm developers (Pappenberger et al., 2007a).

The primary advantage of crowd-sourcing is that calibration points can be in the floodplains (Van Wesemael et al., 2019), where settlements usually exist rather than just in the channel, as it should not be assumed that a hydraulic model well calibrated in the channel will perform equally well in the floodplains (Pappenberger et al., 2007b). Crowd-sourced water levels therefore provide a unique opportunity to calibrate the model diagnostic variables in those areas where accurate estimates of flow and depth are required (Assumpção et al., 2018). In future, they may serve as complementary datasets to support remote sensing based model calibration (e.g., Tarpanelli et al., 2013; Domeneghetti et al., 2014; Wood et al., 2016; Dasgupta et al., 2020), especially to address the gaps of satellite data for such applications (see Grimaldi et al., 2016).

5.3. Model validation

Interestingly, comparisons with the observed flood map yield very limited misses but a large number of false alarms. This might be related to the timing of acquisition of the SPOT-6 image (Fig. 3). As the image is acquired towards the end of the hydrograph, the valley is already full and maximum inundation has been achieved. In such a scenario, the hydraulic flood inundation models should rarely miss many flooded pixels. If rising limb images were acquired, when flows are transitioning between the channel and the floodplains, the number of misses and false alarms might be more comparable in the contingency maps.

The inset table in the left panel of Fig. 14 shows a summary of the pixel statistics. The number of correctly identified inundated pixels is substantially larger than the misses and false alarms as noted before. It is expected that the ratio of false alarms is unrealistically high, due to the misclassification of flooding under vegetation in the optical image, which is able to observe only tree canopies. In order to corroborate this hypothesis, the NDVI was calculated to facilitate a qualitative comparison. The right panel of Fig. 14 shows the area identified as "False Alarms" drawn on a base layer of the SPOT-6 NDVI-based vegetation classes. As expected, most of the false alarms were perhaps flooded vegetation pixels not classified as water due to limitations of NDWI-based surface water extraction from optical images.

In spite of the limitations outlined earlier, a Critical Success Index (CSI) value of 0.65 was obtained, which is in the acceptable range for flood modelling and mapping exercises (Wood et al., 2016; Landuyt et al., 2018). The CSI score was found to be slightly biased towards overprediction, catchment size, and event magnitude (Wealands et al., 2005; Stephens et al., 2014; Stephens & Bates 2015). However, as the aim was to verify the model calibration in the Clarence Catchment for a single event, it was used here due to its ubiquity in flood science literature. The model parameterization was therefore considered to be adequate based on this analysis.

6. Conclusions and outlook

This study presents the first attempt towards the use of crowd-sourced water levels for a quantitative calibration of a 2D-hydraulic flood inundation model. The channel roughness parameter for the hydraulic model Lisflood-FP was calibrated using a collection of 32 distributed floodplain water levels, derived from crowd-sourced field photographs of high water marks whose timing of acquisition was unknown. Assuming that these were representative of the maximum water depth observed at each pixel, quantitative performance measures were used to estimate absolute and relative model errors. As a first step of model verification, the calibrated parameter value was inter-compared

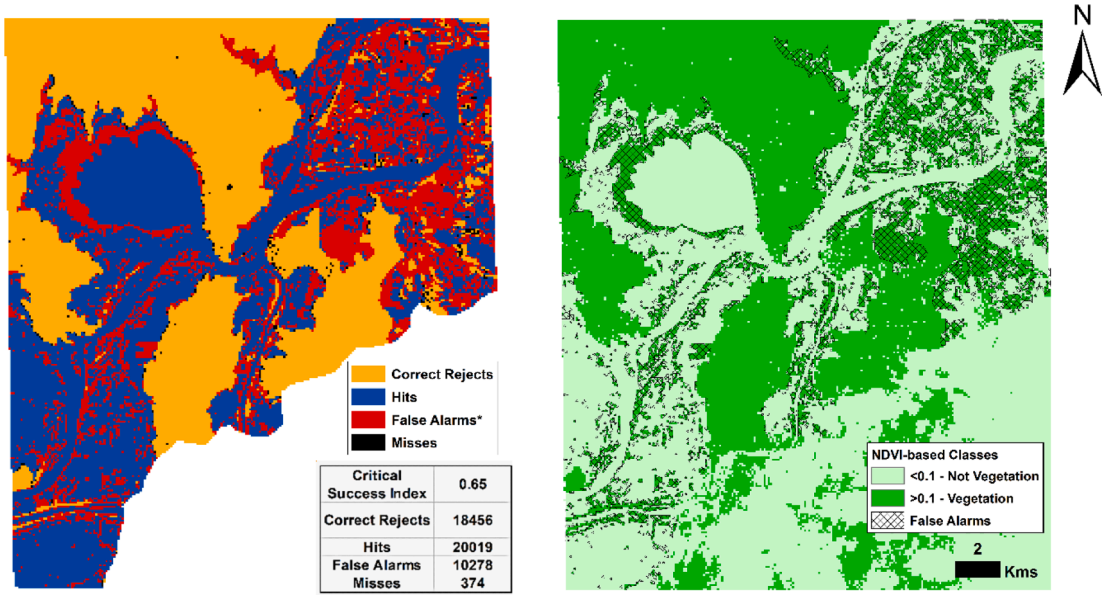

Fig. 14. The left panel shows the contingency map and statistics comparing the surface water extent map based on NDWI values derived from the SPOT-6 optical image against the inundation extents simulated by the LISFLOOD-FP acceleration solver in full 2D using the calibrated channel roughness parameter. False Alarms* indicates a lack of confidence in the inundation identified through the SPOT-6 image due to dense vegetation. The right panel shows the NDVI map indicating area covered by vegetation and not vegetated regions, with respect to the extent of the False Alarms obtained.

with similar information derived from hydrometric gauges, which revealed that crowd-sourcing could be a viable data collection option. Furthermore, plots of maximum water depth simulated by the calibrated model were compared against those obtained through crowd-sourcing and gauges, revealing only minimal deviations from the observations. Finally, the inundation extent simulated by the calibrated model was evaluated against an optical remote sensing image, demonstrating acceptable agreement with the reliable surface water estimates extractable from the RS data.

This study showed that it is possible to use a limited number of accurate crowd-sourced water levels to constrain a 2D-hydraulic model, especially in ungauged or flashy catchments where remote sensing data is limited. The methods developed in this paper can easily be extended to large volumes of crowd-sourced data, albeit the availability of an associated time stamp and geolocation is necessary. In case of slight uncertainties in the timing, approaches suggested by Hostache et al. (2009) could be used, where the model is forced to lie within observation error limits rather than replicate the measurements. In the presence of geolocation errors, the approach of (Schumann and Pappenberger, 2008) should be used to shift the pixel randomly in all directions within the limits of the horizontal accuracy, to derive a range of possible uncertain values which can then be utilised together with the aforementioned technique.

Many research questions still remain, such as how to objectively account for larger uncertainties or how to automatically derive water levels from crowd-sourced images accounting for all uncertainties. However, through this study a simple framework was developed and tested, being capable of ingesting crowd-sourced water levels after a preliminary quality check (Fohringer et al., 2015), successfully demonstrating their utility for flood model performance assessment.

CRediT authorship contribution statement

Antara Dasgupta: Conceptualization, Formal analysis, Investigation, Methodology, Software, Validation, Visualization, Writing – original draft. **Stefania Grimaldi:** Data curation, Investigation, Writing – review & editing. **Raaj Ramsankaran:** Supervision, Writing – review & editing. **Valentijn R.N. Pauwels:** Funding acquisition, Writing – review & editing. **Jeffrey P. Walker:** Conceptualization, Funding acquisition, Supervision, Writing – review & editing.

Declaration of Competing Interest

The authors declare that they have no known competing financial interests or personal relationships that could have appeared to influence the work reported in this paper.

Data availability

The authors do not have permission to share data.

Acknowledgements

This study was conducted within the framework of the project “Improving flood forecast skill using remote sensing data,” funded by the Bushfire and Natural Hazards CRC of Australia. Additionally, gratitude is extended to the Australian Bureau of Meteorology (http://www.bom.gov.au/waterdata/) and New South Wales Manly Hydraulics Laboratory (http://new.mhl.nsw.gov.au/) for the gauge data, in addition to Geoscience Australia and the Clarence Valley Council for sharing field and ancillary data. Antara Dasgupta was funded by a PhD scholarship from the IITB-Monash Research Academy and a Postdoctoral Scholarship from the University of Osnabrück.

References

Andreadis, K.M., Schumann, G.J.P. 2014. Estimating the impact of satellite observations on the predictability of large-scale hydraulic models. Adv. Water Resour. [Internet]. [accessed 2014 Aug 11] 73:44–54. http://linkinghub.elsevier.com/retrieve/pii/S0309170814001158.

Annis, A., Nardi, F., 2019. Integrating VGI and 2D hydraulic models into a data assimilation framework for real time flood forecasting and mapping. Geo-Spatial Inf. Sci. [Internet]. 22 (4), 223–236. https://doi.org/10.1080/10095020.2019.1626135.

Arcement, G.J., Schneider, V.R. 1989. Guide for Selecting Manning ' s Roughness Coefficients for Natural Channels and Flood Plains United States Geological Survey Water-supply Paper 2339 [Internet]. [place unknown]. http://www.fhwa.dot.gov/BRIDGE/wsp2339.pdf.

Assumpção, T.H., Popescu, I., Jonoski, A., Solomatine, D.P., 2018. Citizen observations contributing to flood modelling: opportunities and challenges. Hydrol. Earth Syst. Sci. 22, 1473–1489.

Astrium Services, 2013. SPOT 6 & SPOT 7 imagery user guide. Astrium Serv. 77.

Beven, K., 2006. A manifesto for the equifinality thesis. J. Hydrol. 320 (1–2), 18–36.

Chaudhary, P., D'Aronco, S., Moy De Vitry, M., Leitão, J.P., Wegner, J.D., 2019. Flood-water level estimation from social media images. ISPRS Ann Photogramm Remote Sens Spat Inf. Sci. 4 (2/W5), 5–12.

Chaudhary, P., D'Aronco, S., Leitão, J.P., Schindler, K., Wegner, J.D., 2020. Water level prediction from social media images with a multi-task ranking approach. ISPRS J. Photogramm. Remote Sens. [Internet]. 167 (July), 252–262. https://doi.org/10.1016/j.isprsjprs.2020.07.003.

Cohen, J., 1960. A coefficient of agreement for nominal scales. Educ. Psychol. Meas. 20 (1), 37–46.

Dasgupta, A., Thakur, P.K., Gupta, P.K., 2020. Potential of SAR-derived flood maps for hydrodynamic model calibration in data scarce regions. J. Hydrol. Eng. [Internet]. 25 (9), 05020028. http://ascelibrary.org/doi/10.1061/%28ASCE%29HE.1943-5584.0001988.

DFSI, Spatial Services, A Division of Department of Finance, Services and Innovation, Government of Australia, 2010. Available from https://s3-ap-southeast-2.amazonaws.com/nsw.elvis/z56/Metadata/Barepoint201004-LID1-AHD_5006712_56_0002_0002_1m_Metadata.html# accessed on 03-10-2022.

Di Baldassarre, G., Schumann, G., Bates, P., 2009. Near real time satellite imagery to support and verify timely flood modelling. Hydrol. Process [Internet]. 23 (5), 799–803. http://jamsb.austms.org.au/courses/CSC2408/semester3/resources/ldp/abs-guide.pdf.

Domeneghetti, A., Tarpanelli, A., Brocca, L., Barbetta, S., Moramarco, T., Castellarin, A., Brath, A., 2014. The use of remote sensing-derived water surface data for hydraulic model calibration. Remote Sens. Environ. 149, 130–141.

Farr, A., Huxley, C. 2013. Lower Clarence Flood Model Update 2013. [place unknown].

Donaldson, R.J., Dyer, R.M., Kraus, M.J., 1975. An objective evaluator of techniques for predicting severe weather events. In: *Preprints, Ninth Conf. on Severe Local Storms*, Vol. 321326. Amer. Meteor. Soc, Norman, OK.

Fohringer, J., Dransch, D., Kreibich, H., Schroter, K., 2015. Social media as an information source for rapid flood inundation mapping. Nat. Hazards Earth Syst. Sci. 15 (12), 2725–2738.

Giustarini, L., Matgen, P., Hostache, R., Montanari, M., Plaza, D., Pauwels, V.R.N., De Lannoy, G.J.M., De Keyser, R., Pfister, L., Hoffmann, L., Savenije, H.H.G., 2011. Assimilating SAR-derived water level data into a hydraulic model: a case study. Hydrol. Earth Syst. Sci. [Internet] 15 (7), 2349–2365.

Grimaldi, S., Li, Y., Walker, J.P., Pauwels, V.R.N., 2018. Effective representation of river geometry in hydraulic flood forecast models. Water Resour. Res. [Internet].

Grimaldi, S., Li, Y., Pauwels, V.R.N., Walker, J.P., 2016. Remote sensing-derived water extent and level to constrain hydraulic flood forecasting models: opportunities and challenges. Surv. Geophys. [Internet]. 37 (5), 977–1034. http://link.springer.com/10.1007/s10712-016-9378-y.

Gupta, H.V., Kling, H., Yilmaz, K.K., Martinez, G.F., 2009. Decomposition of the mean squared error and NSE performance criteria: implications for improving hydrological modelling. J. Hydrol. [Internet]. 377 (1–2), 80–91. https://doi.org/10.1016/j.jhydrol.2009.08.003.

Horritt, M.S., Bates, P.D., 2001. Effects of spatial resolution on a raster based model of flood flow. J. Hydrol. 253.

Hostache, R., Matgen, P., Schumann, G., Puech, C., Hoffmann, L., Pfister, L., 2009. Water level estimation and reduction of hydraulic model calibration uncertainties using satellite SAR images of floods. IEEE Trans. Geosci. Remote Sens. [Internet] 47 (2), 431–441. http://ieeexplore.ieee.org/document/4773470/.

Hostache, R., Chini, M., Giustarini, L., Neal, J., Kavetski, D., Wood, M., Corato, G., Pelich, R., Matgen, P., 2018. Near-real-time assimilation of SAR-derived flood maps for improving flood forecasts. Water Resour. Res. [Internet]. 54 (8), 5516–5535. https://onlinelibrary.wiley.com/doi/abs/10.1029/2017WR022205.

Huxley, C., Beaman, F. 2014. Additional crossing of the Clarence River at Grafton: flood impact, levee upgrade, and structural considerations. In: Hydraul Struct Soc - Eng challenges Extrem [Internet]. Brisbane, Australia; p. 1–8. http://espace.library.uq.edu.au/view/UQ:329700.

Jain, S.K., Singh, R.D., Jain, M.K., Lohani, A.K., 2005. Delineation of flood-prone areas using remote sensing techniques. Water Resour. Manag. 19 (4), 333–347.

Jarlan, L., Mangiarotti, S., Mougin, E., Mazzega, P., Hiernaux, P., Le Dantec, V., 2008. Assimilation of SPOT/VEGETATION NDVI data into a sahelian vegetation dynamics model. Remote Sens. Environ. 112 (4), 1381–1394.

Jung, H.C., Jasinski, M., Kim, J.-W., Shum, C.K., Bates, P., Neal, J., Lee, H., Alsdorf, D., 2012. Calibration of two-dimensional floodplain modeling in the central Atchafalaya Basin Floodway System using SAR interferometry. Water Resour. Res. [Internet] 48 (7).

Kutija, V., Bertsch, R., Glenis, V., Alderson, D., Parkin, G., Walsh, C.L., Robinson, J., Kilsby, C. 2014. Model Validation Using Crowd-Sourced Data From a Large Pluvial Flood. 11th Int. Conf. Hydroinformatics:9.

Landuyt, L., Van Wesemael, A., Schumann, G.-J.-P., Hostache, R., Verhoest, N.E.C., Van Coillie, F.M.B., 2018. Flood mapping based on synthetic aperture radar: an assessment of established approaches. IEEE Trans. Geosci. Remote Sens. [Internet] 1–18. https://ieeexplore.ieee.org/document/8432448/.

Le Boursicaud, R., Pénard, L., Hauet, A., Thollet, F., Le Coz, J., 2016. Gauging extreme floods on YouTube: application of LSPIV to home movies for the post-event determination of stream discharges. Hydrol. Process. 30 (1), 90–105.

Le Coz, J., Patalano, A., Collins, D., Guillén, N.F., García, C.M., Smart, G.M., Bind, J., Chiaverini, A., Le Boursicaud, R., Dramais, G., Braud, I., 2016. Crowdsourced data for flood hydrology: feedback from recent citizen science projects in Argentina, France and New Zealand. J. Hydrol. [Internet]. 541, 766–777. https://doi.org/10.1016/j.jhydrol.2016.07.036.

Lopez, T., Al Bitar, A., Biancamaria, S., Güntner, A., Jäggi, A., 2020. On the use of satellite remote sensing to detect floods and droughts at large scales. Surv. Geophys. [Internet] 41 (6), 1461–1487. https://doi.org/10.1007/s10712-020-09618-0.

Lu, S., Wu, B., Yan, N., Wang, H., 2011. Water body mapping method with HJ-1A/B satellite imagery. Int. J. Appl. Earth Obs. Geoinf. [Internet]. 13 (3), 428–434. https://doi.org/10.1016/j.jag.2010.09.006.

Mason, D.C., Cobby, D.M., Horritt, M.S., Bates, P.D., 2003. Floodplain friction parameterization in two-dimensional river flood models using vegetation heights derived from airborne scanning laser altimetry. Hydrol. Process. 17 (9), 1711–1732.

Mazzoleni, M., Alfonso, L., Chacon-Hurtado, J., Solomatine, D., 2015. Assimilating uncertain, dynamic and intermittent streamflow observations in hydrological models. Adv. Water. Resour. [Internet]. 83 (August), 323–339. http://linkinghub.elsevier.com/retrieve/pii/S0309170815001517.

Mazzoleni, M., Chacon-Hurtado, J., Noh, S.J., Seo, D.-J., Alfonso, L., Solomatine, D., 2018. Data assimilation in hydrologic routing: impact of model error and sensor placement on flood forecasting. J. Hydrol. Eng. [Internet]. 23 (6), 04018018. https://ascelibrary.org/doi/pdf/10.1061/%28ASCE%29HE.1943-5584.0001656%0Ahttp://ascelibrary.org/doi/10.1061/%28ASCE%29HE.1943-5584.0001656.

McFeeters, S.K., 1996. The use of the Normalized Difference Water Index (NDWI) in the delineation of open water features. Int. J. Remote Sens. 17 (7), 1425–1432.

McFeeters, S.K., 2013. Using the normalized difference water index (ndwi) within a geographic information system to detect swimming pools for mosquito abatement: a practical approach. Remote Sens. 5 (7), 3544–3561.

Mukherjee, N.R., Samuel, C., 2016. Assessment of the temporal variations of surface water bodies in and around Chennai using landsat imagery. Indian J. Sci. Technol. 9 (18).

Mukolwe, M.M., Yan, K., Di Baldassarre, G., Solomatine, D.P., 2016. Testing new sources of topographic data for flood propagation modelling under structural, parameter and observation uncertainty. Hydrol. Sci. J. 61 (9), 1707–1715.

Nardi, F., Cudennec, C., Abrate, T., Allouch, C., Annis, A., Assumpção, T., Aubert, A.H., Bérod, D., Braccini, A.M., Buytaert, W., et al., 2021. Citizens AND HYdrology (CANDHY): conceptualizing a transdisciplinary framework for citizen science addressing hydrological challenges. Hydrol. Sci. J. [Internet]. 00 (00), 1–18. https://doi.org/10.1080/02626667.2020.1849707.

NLWRA NL and WRA. 2000. Australian Water Resource Assessment. [place unknown].

Pappenberger, F., Beven, K., Horritt, M., Blazkova, S., 2005. Uncertainty in the calibration of effective roughness parameters in HEC-RAS using inundation and downstream level observations. J. Hydrol. [Internet] 302 (1–4), 46–69.

Pappenberger, F., Beven, K., Frodsham, K., Romanowicz, R., Matgen, P., 2007a. Grasping the unavoidable subjectivity in calibration of flood inundation models: a vulnerability weighted approach. J. Hydrol. [Internet] 333 (2–4), 275–287.

Pappenberger, F., Frodsham, K., Beven, K.J., Romanovicz, R., Matgen, P., 2007b. Fuzzy set approach to calibrating distributed flood inundation models using remote sensing observations. Hydrol. Earth Syst. Sci. [Internet]. 11 (2), 739–752. http://www.hydrol-earth-syst-sci.net/11/739/2007/.

Paul, J.D., Buytaert, W., Allen, S., Ballesteros-Cánovas, J.A., Bhusal, J., Cieslik, K., Clark, J., Dugar, S., Hannah, D.M., Stoffel, M., et al., 2018. Citizen science for hydrological risk reduction and resilience building. Wiley Interdiscip. Rev Water. 5 (1), e1262.

Prestininzi, P., Di Baldassarre, G., Schumann, G., Bates, P.D., 2011. Selecting the appropriate hydraulic model structure using low-resolution satellite imagery. Adv. Water Resour. [Internet]. 34 (1), 38–46. https://doi.org/10.1016/j.advwatres.2010.09.016.

Rogencamp, G. 2004. Lower Clarence River Flood Study Review – Final Report: March 2004: Volume 1 of 2 Main Text. [place unknown].

Schnebele, E., Cervone, G., Waters, N., 2014. Road assessment after flood events using non-authoritative data. Nat. Hazards Earth Syst. Sci. [Internet]. 14 (4), 1007–1015. http://www.nat-hazards-earth-syst-sci.net/14/1007/2014/nhess-14-1007-2014.html.

Schumann, G., Pappenberger, F., Matgen, P., 2008. Estimating uncertainty associated with water stages from a single SAR image. Adv. Water Resour. [Internet] 31 (8), 1038–1047.

Schumann, G., Matgen, P., Hoffmann, L., Hostache, R., Pappenberger, F., Pfister, L., 2007. Deriving distributed roughness values from satellite radar data for flood inundation modelling. J. Hydrol. [Internet] 344 (1–2), 96–111.

See, L., 2019. A review of citizen science and crowdsourcing in applications of pluvial flooding. Front. Earth Sci. 7 (March), 1–7.

See, L., Fritz, S., Dias, E., Hendriks, E., Mijling, B., Snik, F., Stammes, P., Vescovi, F.D., Zeug, G., Mathieu, P.P., et al., 2016. Supporting earth-observation calibration and validation: a new generation of tools for crowdsourcing and citizen science. IEEE Geosci. Remote Sens. Mag. 4 (3), 38–50.

Shaad, K., Ninsalam, Y., Padawangi, R., Burlando, P., 2016. Towards high resolution and cost-effective terrain mapping for urban hydrodynamic modelling in densely settled river-corridors. Sustain. Cities Soc. [Internet]. 20, 168–179. https://doi.org/10.1016/j.scs.2015.09.005.

Sinclair Knight Merz, F., Roads and Traffic Authority of NSW TPS. 2011. Wells Crossing to Iluka Road: upgrading the Pacific Highway: Tyndale to Maclean alternative alignment: decision report. [place unknown].

Stephens, E., Bates, P., 2015. Assessing the reliability of probabilistic flood inundation model predictions. Hydrol. Process [Internet]. http://doi.wiley.com/10.1002/hyp.10451.

Stephens, E., Schumann, G., Bates, P., 2014. Problems with binary pattern measures for flood model evaluation. Hydrol. Process. 28 (18), 4928–4937.

Sunkara, V., Purri, M., Saux, B. Le, Adams, J. 2020. Street to Cloud: Improving Flood Maps With Crowdsourcing and Semantic Segmentation. In: NeurIPS2020 [Internet]. [place unknown]; p. 1–5. http://arxiv.org/abs/2011.08010.

Tarpanelli, A., Brocca, L., Melone, F., Moramarco, T., 2013. Hydraulic modelling calibration in small rivers by using coarse resolution synthetic aperture radar imagery. Hydrol. Process. 27 (9), 1321–1330.

Tellman, B., Lall, U., Islam, A.K.M.S., Bhuyan, M.A., 2022. Regional index insurance using satellite-based fractional flooded area. Earth's Futur. 10 (3).

Van Wesemael, A., Landuyt, L., Lievens, H., Verhoest, N.E.C., 2019. Improving flood inundation forecasts through the assimilation of in situ floodplain water level measurements based on alternative observation network configurations. Adv. Water Resour. [Internet]. 130 (January), 229–243. https://doi.org/10.1016/j.advwatres.2019.05.025.

Wang, Y., Ruan, R., She, Y., Yan, M., 2011. Extraction of water information based on RADARSAT SAR and Landsat ETM+. Procedia Environ. Sci. [Internet] 10 (PART C), 2301–2306. https://doi.org/10.1016/j.proenv.2011.09.359.

Wealands, S.R., Grayson, R.B., Walker, J.P., 2005. Quantitative comparison of spatial fields for hydrological model assessment - Some promising approaches. Adv. Water Resour. 28 (1), 15–32.

Werner, M.G.F., Hunter, N.M., Bates, P.D., 2005. Identifiability of distributed floodplain roughness values in flood extent estimation. J. Hydrol. [Internet] 314 (1–4), 139–157.

Wing, O.E.J., Bates, P.D., Sampson, C.C., Smith, A.M., Johnson, K.A., Erickson, T.A., 2017. Validation of a 30 m resolution flood hazard model of the conterminous United States. Water Resour. Res. 53 (9), 7968–7986.

Wood, M., Hostache, R., Neal, J., Wagener, T., Giustarini, L., Chini, M., Corato, G., Matgen, P., Bates, P., 2016. Calibration of channel depth and friction parameters in the LISFLOOD-FP hydraulic model using medium-resolution SAR data and identifiability techniques. Hydrol. Earth Syst. Sci. 20 (12), 4983–4997.

Ye, W., Hansen, D.P., Jakeman, A.J., Sharma, P., Cooke, R., 1997. Assessing the natural variability of runoff: Clarence Basin catchments, NSW, Australia. Math. Comput. Simul. [Internet]. 43 (3–6), 251–260. http://www.sciencedirect.com/science/article/B6V0T-3SP2CCR-3/2/2ab91a85f51787e7c9fa88de185219bc.

Yu, D., Yin, J., Liu, M., 2016. Validating city-scale surface water flood modelling using crowd- sourced data. Environ. Res. Lett. 11, 1748–9326.

Zhang, X., Beeson, P., Link, R., Manowitz, D., Izaurralde, R.C., Sadeghi, A., Thomson, A.M., Sahajpal, R., Srinivasan, R., Arnold, J.G., 2013. Efficient multi-objective calibration of a computationally intensive hydrologic model with parallel computing software in Python. Environ. Model Softw. 46, 208–218.